PHYSICAL REVIEW B VOLUME 22, NUMBER 7 1 OCTOBER 1980

Nuclear quadrupole resonance studies of amorphous, orthorhombic, and rhombohedral arsenic

G. E. Jellison, Jr.
Solid State Division, Oak Ridge National Laboratory, Oak Ridge, Tennessee 37830*

G. L. Petersen
Matec, Incorporated, Warwick, Rhode Island 02886

P. C. Taylor
Naval Research Laboratory, Washington, D. C. 20375

(Received 14 April 1980)

Pulsed nuclear quadrupole resonance (NQR) experiments have been performed on three forms of elemental arsenic: amorphous (*a*), rhombohedral (*rh*), and orthorhombic (*or*). The temperature dependence of the spin-lattice relaxation time (T_1) provides evidence for the existence of disorder (tunneling) modes in *a*-As. It is found that the NQR line shape of *a*-As is highly asymmetric, and this asymmetry is attributed to a distribution of dihedral angles in *a*-As. The observed NQR frequencies indicate that the amount of bonding *s* admixture is different in each material (*rh*-As:3%, *or*-As:7%, *a*-As:10%). Simple calculations in comparison with x-ray results indicate that the bonding configurations in these three forms of arsenic do not necessarily correspond to maximum overlap of bonding orbitals on adjacent atoms.

I. INTRODUCTION

Amorphous arsenic (*a*-As) is of particular interest as a prototype amorphous solid for two reasons. First of all, since *a*-As is an elemental solid, its structural and electronic properties should be easier to understand than those of more chemically complex amorphous solids, such as most of the chalcogenide glasses. Second, all atoms in *a*-As are threefold coordinated; this coordination in arsenic falls between the tetrahedrally coordinated amorphous solids, such as *a*-Ge and *a*-Si, and the chalcogenide glasses in which the chalcogen elements (S, Se, Te) are predominantly twofold coordinated. Therefore, due to its threefold coordination, many of the structural and electronic properties of *a*-As have characteristics similar to those observed in both group-IV and in group-VI amorphous solids.[1]

The similarities and differences between the properties of *a*-As and group-IV or group-VI amorphous solids are emphasized by the results of several experiments. First of all, the infrared and Raman vibrational spectra[2,3] in *a*-As reflect predominantly the phonon density of states[4] as is the case in *a*-Ge and *a*-Si. There is, however, some evidence for effects due to the different Raman and infrared matrix elements as one observes in the chalcogenides.[2,5-7] Secondly, the linear term in the low-temperature specific heat, which is present in all chalcogenide and oxide glasses[8] but absent in *a*-Ge,[9] is at least an order of magnitude smaller in *a*-As than in the chalcogenides.[10] However, as we shall demonstrate below, there is evidence[11] from the spin-lattice relaxation time (T_1) measurements of ^{75}As for the existence of disorder or tunneling modes in *a*-As, such as those contributing to the linear specific heat. Finally, some of the defects observed by photoluminescence (PL) or optically induced ESR in *a*-As are similar to those encountered in the chalcogenide glasses,[12] but additional defects are also observed.[13] Some weak features in the Raman and infrared spectra of *a*-As have been attributed to defects,[14] but there is no evidence for counterparts in the spectra of the chalcogenides.

Nuclear quadrupole resonance (NQR) is a useful probe of local order which is often very sensitive to small changes in the immediate environment; however, due to the weak signals observed in amorphous solids this technique has been rarely used to study these materials. The only previous NQR results of an amorphous solid are the ^{75}As pulsed measurements of Rubinstein and Taylor[15] on As_2S_3 and As_2Se_3. These previous measurements include the NQR line shape and the temperature dependence of the spin-lattice and spin-spin relaxation times, T_1 and T_2, respectively. From the line-shape results, it was concluded that the AsS_3 and $AsSe_3$ pyramidal units were well preserved in the glasses, and that they resembled those occurring in the corresponding crystalline solids. The T_1 data were interpreted as evidence for the existence of tunneling modes in these glasses. Recent ^{11}B pulsed nuclear magnetic resonance (NMR) data[16,17] in B_2O_3 glass have also been interpreted[18,19] in terms of Raman processes involving tunneling modes, although the exact mechanism is still a matter of some debate.[18,19] The T_2 data were analyzed by Rubinstein and Tay-

lor[15] in terms of a dipolar dephasing between like arsenic nuclei. Recently Szeftel and Alloul[20] have employed a novel pulsed NMR technique to determine the asymmetry in the quadrupolar interaction of ^{75}As in vitreous As_2Se_3. They find two sites in the glass, one of which does not appear to coincide with any sites occurring in crystalline As_2Se_3.

In general, NQR and NMR (on nuclei with nuclear spin $I > \frac{1}{2}$) techniques as applied to amorphous solids provide very sensitive probes of local structure and electronic bonding from the observed NQR and NMR line shapes. Measurements of T_1 provide a probe of low-frequency excitations in amorphous solids, and measurements of T_2 give information on separations between mutually resonant nuclei and perhaps on such esoteric mechanisms as nuclear-spin diffusion.[21] This information is even more useful when direct comparisons can be made between glasses and crystals of the same chemical composition.

In this paper we present pulsed NQR measurements of ^{75}As in three solid forms of arsenic: *a*-As, orthorhombic arsenic (*or*-As), and rhombohedral arsenic (*rh*-As). The local environment in all three forms is very similar in that each As atom is threefold coordinated in a bonding arrangement which has a local three-dimensional character. In the common, semimetallic crystalline form[22] (*rh*-As) the layers are formed which are of semi-infinite extent and are composed of six-member rings in which the As atoms are aligned in a staggered configuration [see Fig. 1(b)]. In the less common, semiconducting crystalline form[23] (*or*-As) layers are formed with six-member rings which are composed of As atoms in a "semistaggered" or "chair" configuration [see Fig. 1(a)]. The detailed structure of *a*-As is not known, but continuous random network (CRN) models[24,25] suggest that both the local three-dimensional character and some vestiges of the quasi-two-dimensional ring structure remain. The ^{75}As NQR measurements on those forms of arsenic are consistent with these general structural features. The NQR results of *a*-As provide experimental evidence for second-nearest-neighbor structural correlations which are implicit in the CRN models from variations of the dihedral angle.

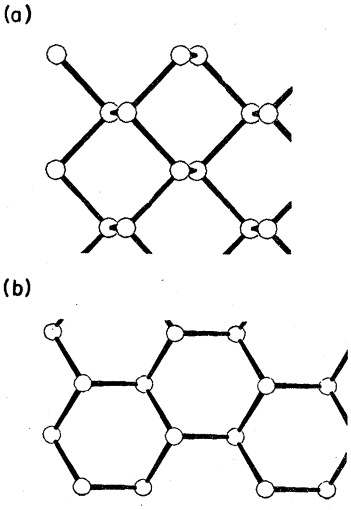

FIG. 1. Projections of atomic layers found in two crystalline forms of arsenic: (a) projection along the [100] direction of orthorhombic arsenic; (b) projection along the [111] direction of rhombohedral arsenic.

In Sec. II we present a brief summary of those theoretical concepts necessary to understand the pulsed NQR experiments. Sections III and IV describe the experimental procedure and results, respectively. The spin-lattice and spin-spin relaxation measurements in *a*-As are discussed in Sec. V. Section VI describes the local bonding information which can be inferred from the NQR line shape. Finally, the results are summarized in Sec. VII.

II. NQR BACKGROUND AND THEORY

Nuclear quadrupole resonance (NQR) spectroscopy has been used for many years as a sensitive probe of local electronic structure. As the theory is well developed and given in standard texts,[26,27] only a brief explanation of NQR will be presented here.

The nucleus ^{75}As is 100% naturally abundant and possesses a spin $I = \frac{3}{2}$. Since this spin is greater than $\frac{1}{2}$, the ^{75}As nucleus also possesses a nuclear quadrupole moment (Q). This quadrupole moment interacts with the electric-field gradient (EFG) at the site of the nucleus and results (for the case of $I = \frac{3}{2}$) in two doubly degenerate energy levels given by

$$E_{\pm} = \pm (Q_{cc}/4) h (1 + \eta^2/3)^{1/2} , \tag{1}$$

where Q_{cc} is the quadrupole coupling constant ($Q_{cc} = e^2 Qq/h$ where $eq = eq_{zz}$ is the component of maximum magnitude of the EFG tensor in the principal axis system), and η is the asymmetry parameter [defined by $(q_{xx} - q_{yy})/q_{zz}$]. The quantity Q_{cc} is a measure of the strength of the quadrupole interaction, while η is a measure of the departure of the EFG tensor from axial symmetry. If the system is in thermal equilibrium, then the populations of the two levels can be determined by Boltzmann statistics for any temperature above 0.1 K.

If the sample is placed in a radio frequency (rf) magnetic field, transitions between these two levels can occur when the frequency of this rf field is

$$\nu = |(E_+ - E_-)/h| = |(Q_{cc}/2)(1+\eta^2/3)^{1/2}| . \quad (2)$$

In general, the transition probability is a function of the angle between the rf field and the principal axis system.

Once the nuclear system is taken out of equilibrium, it will normally return to equilibrium exponentially. The spin-lattice relaxation time (T_1) is a measure of the time it takes to reestablish the Boltzmann distribution, and is therefore a measure of the energy exchange of the spin system and the lattice. The spin-spin relaxation time (T_2) is a measure of the dephasing time of the spin system; this time represents only a change in the entropy of the system and can be thought of as being the characteristic time required for the off-diagonal elements of the density matrix between states of different energy to go to zero.

For the purposes of this paper, we define the following pulsed excitations of the sample: a "90°" ("180°") pulse is of sufficient duration and magnitude to induce just enough transitions to equate (invert) the populations of the E_+ and E_- states. As is conventional we shall henceforth omit the quotation marks from future references to 90° or 180° pulses. For a powdered or glassy sample, the 90° pulse corresponds to the first maximum of the spherical Bessel function $j(\sqrt{3}\omega_1\tau_\omega)$, while the 180° pulse corresponds to the first zero (other than $\tau_\omega = 0$) for this same function (here, $\omega_1 = \gamma H_1$, γ is the gyromagnetic ratio, H_1 is the magnitude of the rf magnetic field, and τ_ω is the pulse width). Therefore the 90° pulse requires $\sqrt{3}\omega_1\tau_\omega = 0.66\pi$, while the 180° pulse requires $\sqrt{3}\omega_1\tau_\omega = 1.43\pi$.

All measurements employed the following pulse sequence[28,29]:

$$90° - \tau - 180° - t - 90° - \tau - 180° - t - \cdots .$$

The application of the first rf pulse results in a transient excitation of the nuclear-spin system, and a response [called the free-induction decay (FID)] is normally observable immediately after the pulse. The application of the second rf pulse leads to a response at time 2τ, which is called the "spin-echo." The duration of the FID is inversely proportional to the linewidth of the NQR; therefore, for the cases of *or*-As and *a*-As (see Sec. IV), no FID was observable due to the large NQR linewidth. The spin-lattice relaxation time T_1 is obtained by observing the height of the spin-echo as a function of the time between each 90° $-\tau-$ 180° pulse sequence (t),[30] while the spin-spin relaxation time T_2 is obtained by observing the height of the spin-echo as a function of τ (assuming that $t \gg T_1$).[28,29] It is found that the height of the echo $M(t)$ is given by the equation (assuming τ is constant)

$$M(t) = M(\infty)(1 - e^{-t/T_1}), \quad (3)$$

where $M(\infty)$ is the height of the signal when $t \gg T_1$. Equation (3) is valid only for exponential decay, which was the case for all decay observed (see Fig. 2). For a constant t, the height of the echo is given by

$$M(2\tau) = M(0)e^{-2\tau/T_2} . \quad (4)$$

Therefore T_1 (or T_2) can be measured by plotting $[M(\infty) - M(t)]/M(\infty)$ [or $M(2\tau)/M(0)$] semilogarithmically versus t (or 2τ) and taking the slopes.

Though it is well known that the ^{75}As nucleus possesses a quadrupole moment, its magnitude is not well determined. We have used the standard value[27] $Q = 0.29$ barn (1 barn $= 10^{-24}$ cm^2), which is accurate to about ±15%.

III. EXPERIMENTAL CONSIDERATIONS

The NQR measurements were made using a MATEC Model 5100 main frame (which employed a MATEC Model 525 gated amplifier for frequencies between 20 and 140 MHz), a MATEC Model 625 broad-band receiver with the appropriate tuned preamplifier, and appropriate auxiliary equipment arranged in a single-coil, phase-detection system. The receiver-preamplifier system output was linear and flat versus frequency over the operating range of the preamplifier. Because the signal to be observed (especially for the case of *a*-As) was so weak, a high-Q circuit was used which resulted in a large receiver recovery time (~150 μsec). The signal was enhanced using a NICOLET 1074 signal average, an SD-77 fast digitizer plug-in, and an SW-77 sweep unit plug-

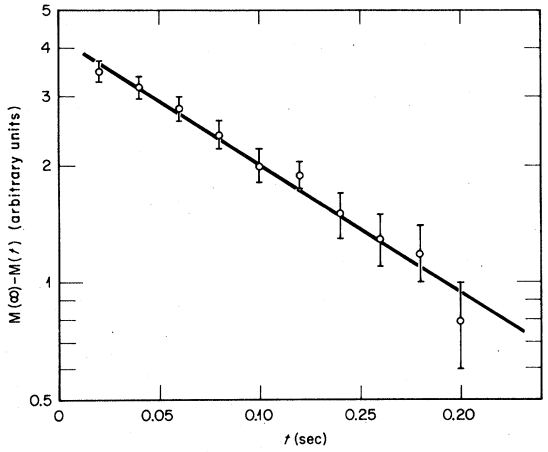

FIG. 2. Spin-lattice relaxation time in *a*-As at 77 K as determined from the normalized magnetization curve (semilogarithmic scale).

in. This signal-averaging system allowed a maximum time resolution of 1 μsec, and a maximum digital signal resolution of 4 bits. Temperatures between 4.2 and 300 K were obtained using a gas flow (either helium or nitrogen) system; temperatures were measured using a copper-constantin thermocouple in intimate contact with the sample.

The data for T_1 and T_2 were measured as described in Sec. II and were fitted by a least-square procedure for all data points to either Eq. (3) or Eq. (4). The line shape (for *a*-As and *or*-As) was obtained by observing the height of the spin echo as a function of operating frequency at constant τ and t. This procedure required tuning the pulser, receiver, and matching network at each frequency and recording the best signal height obtained (after signal averaging for several hundred pulse sequences). This process was not too difficult for the case of *or*-As, since the linewidth is only 340 kHz and only one receiver preamplifier had to be used; however, due to the large range of NQR frequencies two preamplifiers had to be used for the case of *a*-As. Data were taken in an overlap region using both preamplifiers, and the resulting signal heights were then normalized to obtain the entire spectrum. The signal amplification of the active system (preamplifier, amplifier, tuned matching network) was linear in frequency within approximately ±10% over the range investigated. Linearity was checked at selected frequencies by measuring the amplitude of a reference pulse of calibrated intensity which was inserted into a pickup coil (physically well separated from the sample coil).

The samples of *a*-As and *rh*-As (both 99.9999% pure) were obtained from Atomergic Chemetals Corp. (the manufacturer of *a*-As was MCP, Ltd.). Samples of *or*-As were obtained from the Smithsonian Institution (natural mineral arsenolamprite from Chile) and A. J. Leadbetter (synthetically grown and doped with about 2% Hg). X-ray analysis of the natural *or*-As sample indicated that it contained 10–30% *rh*-As. (This was confirmed by NQR studies of the natural *or*-As samples; see Ref. 31.)

IV. RESULTS

The spin-lattice relaxation time T_1, taken as a function of temperature, is shown in Fig. 3 for *a*-As, *or*-As, and *a*-As_2Se_3. In all cases,

$$T_1 \propto T^{-\beta}, \tag{5}$$

where $\beta = 1.5$ for *a*-As, 1.6 for *or*-As, and 1.8 for *a*-As_2Se_3. [T_1 is not shown in Fig. 3 for *rh*-As, but was found to be proportional to T^{-1} (see Ref. 31); the relaxation was attributed to the hyperfine coupling of the ^{75}As nuclei to conduction electrons in the semimetal.] The magnitude of T_1 for *a*-As is about a factor of 3 smaller than T_1 for *or*-As. The filled-in square for *or*-As in Fig. 3 represents the lowest-temperature point taken with the synthetic sample. As was mentioned in Sec. III, this sample contained about 2% Hg; therefore, it is reasonable that the low-temperature relaxation in this sample is due to paramagnetic impurities. The T_1 data for *a*-As_2Se_3 taken below 4.2 K are from Ref. 15, and are represented in Fig. 3 by circles.

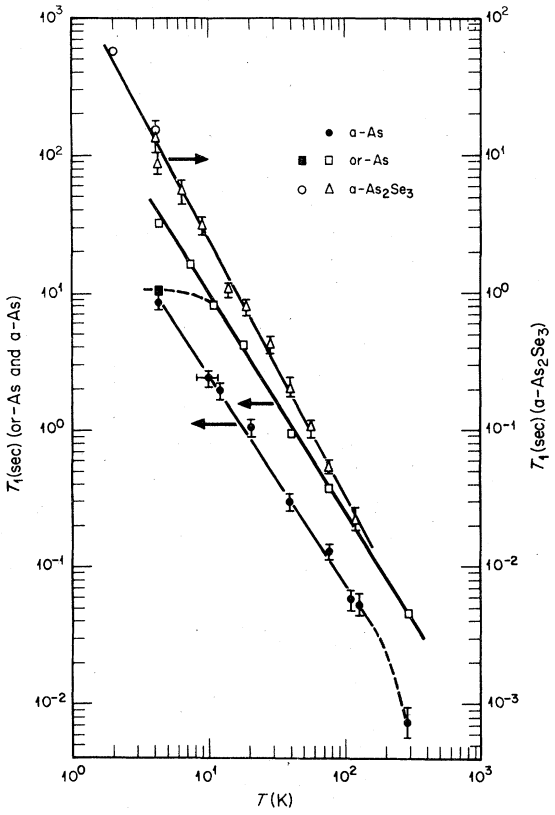

FIG. 3. Spin-lattice relaxation time (T_1) plotted versus temperature for *a*-As, *or*-As, and *a*-As_2Se_3. Note the difference in scale between *or*-As and *a*-As and *a*-As_2Se_3. The filled-in square at 4.2 K for *or*-As was determined using the synthetic *or*-As sample and is discussed in the text. The data for *a*-As_2Se_3 represented by the open circles are from Ref. 15.

At $T = 77$ K, T_1 and T_2 were measured as functions of frequency across the *a*-As line shape; the results are shown in Fig. 4. As can be seen T_1 and T_2 are independent of frequency within experimental error. Also, T_2 was measured as a function of temperature (at $\nu_Q = 63$ MHz); it was found that $T_2 = 200 \pm 20$ μsec and was independent of both T and ν_Q. In *or*-As T_2 was measured to be 170 ± 10 μsec independent of the temperature. Un-

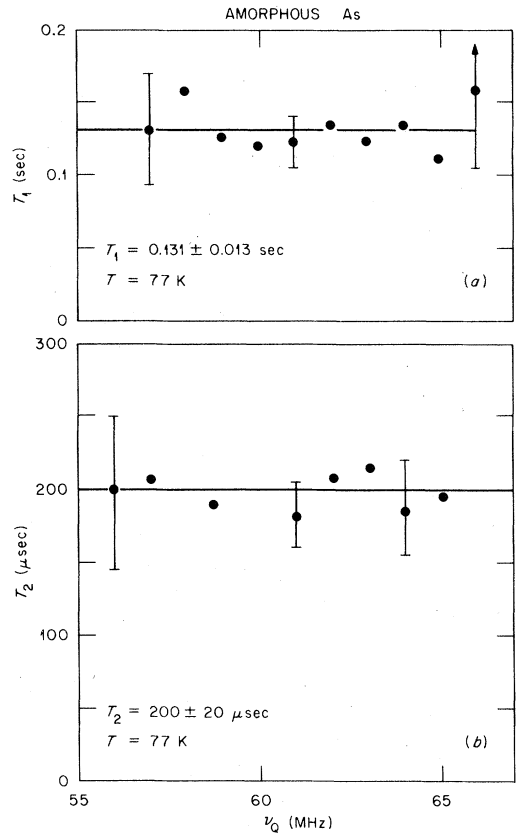

FIG. 4. Spin-lattice (a) and spin-spin (b) relaxation time (T_1, T_2) for ^{75}As NQR at 77 K in a-As as a function of resonant frequency.

like the situation in As_2S_3 and As_2Se_3, the longitudinal relaxation was found to be exponential for both or-As and a-As within experimental accuracy.

Table I lists the central NQR frequency at 4.2 K (ν_Q^0) and the full width at half maximum for the three forms of arsenic, plus the results[15] for a-As_2S_3, c-As_2S_3, a-As_2Se_3, and c-As_2Se_3 for purposes of comparison (a=amorphous, c=crystalline). Also listed in the table are x-ray results[22,23,34,35] of bond angles (α) and bond lengths. Figure 5(a) shows the NQR line shape for a-As at $T=4.2$ K. [Figure 5(b) shows a calculated line shape that will be discussed in Sec. VI.] The experimental line shape was also evaluated at $T=77$ K, but there was no discernible difference between the two temperatures. For comparison, a schematic of the or-As line shape at $T=4.2$ K is included in Fig. 5(a). The NQR line shapes for a- and c-As_2S_3 and As_2Se_3 are shown in Fig. 6 (after Ref. 15). Two features of Figs. 5(a) and 6 must be noted: First of all, the a-As line shape is asymmetric, whereas the line shapes for a-As_2S_3 and a-As_2Se_3 are symmetric within experimental error. Second, the crystalline NQR frequencies for the cases of As_2S_3 and As_2Se_3 fall within the widths at half-height of the amorphous NQR line shape, while this is not the case with a-As; i.e., rh-As, or-As, and a-As all have quite different NQR frequencies.

As was previously found for a-As_2S_3 and a-As_2Se_3,[15] the NQR frequency distribution of a-As was found to be temperature independent. However, the NQR frequencies in rh-As,[32] or-As, and c-As_2S_3 (Ref. 15) exhibit definite temperature dependencies. The temperature dependence of ν_Q^0 for or-As is shown in Fig. 7. This dependence can be explained in terms of torsional vibrations using a simple harmonic oscillator model due to Bayer.[36] In this model

$$\nu = \nu_0[1 - K/\theta_\tau \coth(\theta_\tau/2T)], \tag{6}$$

where K is a constant, and θ_τ is the equivalent temperature of the torsional vibration (the frequency $\nu_\tau = k\theta_\tau/h$). In fitting Eq. (6) to the data in Fig. 7, we obtained $\nu_0^{or}=46.65$ MHz, $K=0.885$ K, and $\nu_\tau = 85 \pm 15$ cm^{-1}; the resulting fit is shown

TABLE I. The central NQR resonant frequency (ν_Q^0), full width at half maximum (FWHM) of the NQR line measured at 4.2 K, arsenic bond angles (α) and bond lengths of the three forms of arsenic, and of amorphous (a) and crystalline (c) As_2S_3 and As_2Se_3. The roman numerals (I and II) after c-As_2S_3 and c-As_2Se_3 refer to the two different sites in the crystals.

	NQR data			X-ray data						
Sample	ν_Q^0 (MHz)	FWHM (MHz)	Ref.	α			Bond lengths (Å)			Ref.
rh-As	23.56	<0.03	32	97.1	97.1	97.1	2.508	2.508	2.508	22
or-As	46.32	0.34		94.1	98.5	98.5	2.49	2.49	2.48	23
a-As	63.5	9.0		~97	~97	~97	2.5	2.5	2.5	23
a-As_2S_3	70.0	7.0	15							
c-As_2S_3 I	72.86	0.1	15	97.1	94.5	106.5	2.21	2.28	2.22	33
II	70.38	0.1	15	95.2	106.1	92.7	2.26	2.26	2.23	33
a-As_2Se_3	57.8	12	15							
c-As_2Se_3 I	56.0	0.1	15	98.2	104.8	95.9	2.37	2.44	2.56	34
II	60.0	0.1	15	102.7	91.8	105.0	2.32	2.37	2.36	34

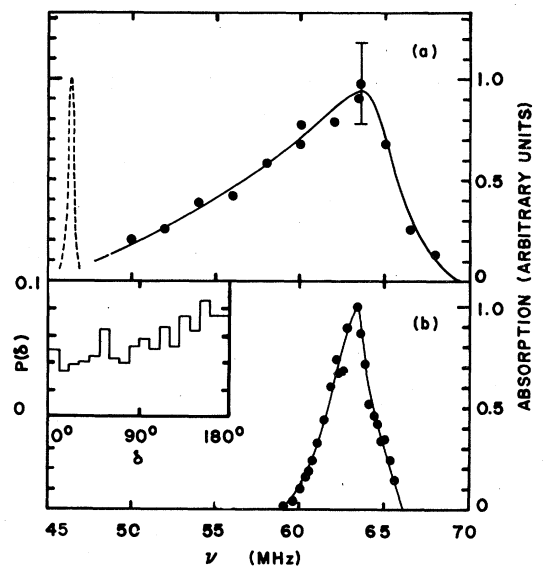

FIG. 5. (a) NQR absorption in amorphous As (circles and solid line) and orthorhombic As (dashed line) at 4.2 K. (b) Calculated contribution to NQR line shape from bonding electrons on nearest-neighbor atoms as described in the text. (The points refer to a calculated histogram through which a smooth curve has been drawn.) Inset: dihedral angle distribution from Ref. 24.

as the solid curve in Fig. 7. Similarly, we have fitted the data of Sharma[32] on *rh*-As with Eq. (6); the resulting parameters are: $\nu_0^{rh}=24.13$ MHz, $K=6.00$ K, and $\nu_\tau=175\pm15$ cm^{-1}.

Figure 8 shows the NQR line shape for *or*-As at 4.2, 77, and 300 K; note that the line shape is asymmetric and rather broad compared to linewidths generally observed in unstrained crystals.

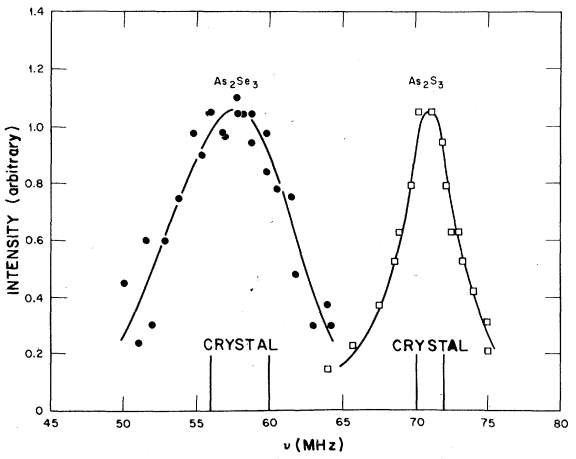

FIG. 6. NQR absorption in amorphous As_2Se_3 and As_2S_3 versus NQR frequency at 4.2 K. The resonant frequencies of the corresponding crystalline materials are shown by the vertical lines (after Ref. 15).

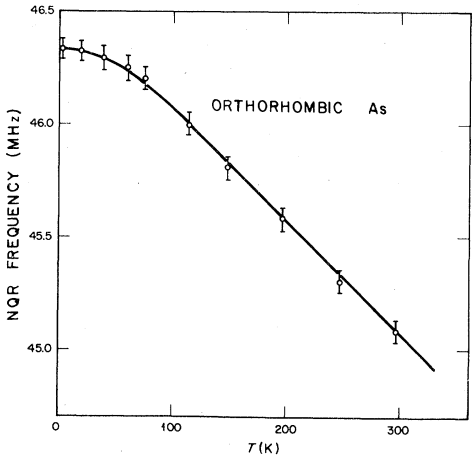

FIG. 7. NQR frequency versus temperature for orthorhombic As. The solid line is the best fit to the data using Eq. (6).

The data in Fig. 8 were taken with the synthetic sample of *or*-As. Similar results were obtained with the natural *or*-As sample, where the resulting linewidth was about 20% less than the synthetic sample. These very broad crystalline lines are not surprising when one considers that both samples are highly strained. These strains lead to a distribution of electric-field gradients at the ^{75}As nuclear sites which creates a broad distribution in NQR frequencies.

V. NUCLEAR-SPIN RELAXATION

A. Spin-lattice relaxation

As described in Sec. II, spin-lattice relaxation is the process by which the magnetization of an ensemble of nuclei approaches thermal equilibrium after excitation by, for example, an appropriate rf pulse of energy. The relaxation process is generally exponential and the inverse of the rate of decay is termed the spin-lattice relaxation time T_1 (see Sec. II). In crystalline solids quadrupolar spin-lattice relaxation results normally from first-order Raman processes involving either acoustic[37] or optical[38] phonons. At low temperatures these two processes depend on the temperature, respectively, as $T_1\propto T^{-7}$ or T^{-9} (acoustic phonons) and $T_1\propto\exp(\epsilon/kT)$, where ϵ is an optical-phonon energy (optical phonons).

In amorphous solids the low-temperature spin-lattice relaxation rates are always dramatically faster than those in corresponding crystalline solids, and the temperature dependences are always weaker ($T_1\propto T^{-\beta}$ where $1\lesssim\beta\lesssim2$). For example, Rubinstein and Taylor[15] found $\beta\cong2$ for As_2S_3 and As_2Se_3. More detailed experimental measurements by the present authors over a wider

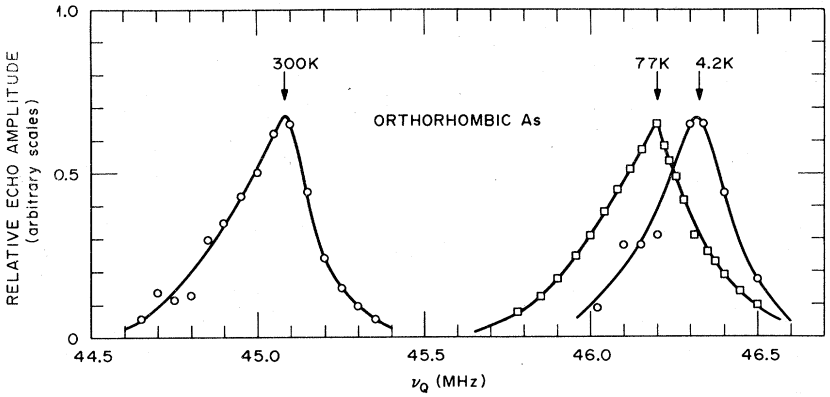

FIG. 8. NQR absorption versus frequency for orthorhombic As at 300, 77, and 4.2 K.

temperature range (see Fig. 3) indicate that $\beta = 1.8 \pm 0.1$ in As_2Se_3. In B_2O_3, $\beta = 1.3$, and in sodium silicate and sodium borate glasses, $\beta = 1.4$ for both the ^{27}Na and ^{11}B nuclei (see Ref. 16). These results are not restricted to quadrupolar nuclei. In calcium phosphate glass, Jellison[39] found that $\beta = 1.0$ at low temperatures even though the nuclear spin of ^{31}P is $\frac{1}{2}$. For protons ($I = \frac{1}{2}$) in various organic glasses, Haupt and Müller-Warmuth[40] obtained values of β between 1.5 and 2.

It is clear that the relaxation processes important for crystalline solids at low temperature are not sufficient to describe the enhanced rates observed in amorphous solids. This situation is not surprising in view of the low-temperature specific-heat measurements[8,41] on amorphous solids which indicate that all amorphous solids exhibit both (1) an "enhanced Debye-type" specific heat ($C_v \propto T^3$) over that which is observed in crystalline counterparts and (2) a linear term in the specific heat ($C_v \propto T$) at the lowest temperatures ($T \lesssim 1$ K) which is not observed in pure crystalline semiconductors or insulators. Other measurements, such as far-infrared and microwave absorption,[42] low-frequency Raman scattering,[43] thermal conductivity,[8,41] also reflect the increased densities of low-frequency vibrational degrees of freedom in amorphous solids.

There is considerable evidence for the existence of modes which are not phonons (not harmonic) from both the linear term in the specific heat[8,41] and low-temperature contributions to the ultrasonic attenuation[44] and microwave dielectric loss,[45] which saturate as functions of microwave power. A model description of these modes (called tunneling or disorder modes) which are peculiar to amorphous solids was suggested by Anderson, Halperin and Varma[46] and by Phillips.[47] This model employs two-level modes with a continuous distribution of energy splittings and appreciable potential barriers between the levels. These modes are considered to arise from the motion of an atom or group of atoms between two positions of local equilibrium which are nearly degenerate in energy. The structural disorder in amorphous solids is invoked to explain the presence of such modes. The tunneling-mode model has been used successfully to explain a variety of physical phenomena in addition to those mentioned above.

The models generally employed to describe spin-lattice relaxation in amorphous solids attribute the observed relaxation to various Raman processes involving tunneling modes and phonons. In their original paper, Rubinstein and Taylor[15] suggested that the spin-lattice relaxation resulted from either a Raman process involving two very-low-frequency phonons or an analog to relaxation by paramagnetic impurities where the role of the "impurity" is played by a tunneling mode. Neither suggestion can explain all the data which are now available; the first explanation cannot yield values of $\beta < 2$ and the second predicts a strong frequency dependence for T_1 which is not observed in pulsed NMR measurements[16,19] (where the frequency can be varied).

Szeftel and Alloul[19] have suggested that at low temperatures T_1 is dominated by a Raman process involving a phonon and a tunneling mode, but Reinecke and Ngai[18] obtain $\beta \geq 4$ for this process. Recently Lyo and Orbach[48] have suggested that this process can yield $\beta \geq 2$ provided that spectral or spin-diffusion processes are taken into account, but these authors are not able to account for values of β less than 2. Spin diffusion in NMR and NQR is the process by which energy is transferred within the nuclear spin system via mutual spin flips of physically close nuclei. Because the tunneling modes are two-level systems they can be described by the long-established formalism for an ensemble of spin-$\frac{1}{2}$ particles, and a mecha-

nism similar to nuclear spin diffusion might also be possible in the tunneling-mode system.[41] Reinecke and Ngai[18] suggested that a Raman process involving two tunneling modes yielded $\beta = 1 + 2\eta$ where η represents the (weak) energy dependence of the density of tunneling modes ($\rho \propto E^{\eta}$). This suggestion has been criticized as being unrealistic[19] because it requires the existence of two tunneling modes with nearly identical energy differences at the same physical location. We believe this criticism is valid, but suggest that "spin-diffusion" within the tunneling-mode system might alleviate this difficulty.

In fact, earlier measurements of Szeftel and Alloul[19] provide an indication of the possible importance of spin diffusion in T_1 processes. In NaB_4O_7 glass, both the ^{23}Na and the ^{11}B nuclei have identical temperature dependences which indicate that they may both sample the same energy-dependent density of tunneling modes. However, the magnitudes of T_1 for these two nuclei do not scale with the square of their respective quadrupole moments, as they should if the coupling were identical in both cases. If the coupling is different, then it is at best fortuitous that both nuclear spin systems couple to densities of tunneling modes which possess the same energy dependence. Spin diffusion in the tunneling-mode system would provide a natural explanation for the same value of β for both ^{23}Na and ^{11}B without the necessity for the coupling to be the same for both nuclei.

Spin diffusion is known to be important in ultrasonic echo experiments in glasses[49,50] where this mechanism dominates the temperature dependence of the tunneling-mode relaxation rate which is analogous to T_1^{-1} in NMR. There is thus some supportive evidence for the existence of spin diffusion in the tunneling-mode system.

Because the Raman process involving two tunneling modes is the only one capable of obtaining the appropriate temperature dependences for T_1, we restrict the present discussion of T_1 in a-As to this process. The weak temperature dependence of T_1 in a-As shown in Fig. 3 strongly indicates the existence in this amorphous solid of very-low-frequency vibrational degrees of freedom which are similar to those present in all other amorphous solids. If tunneling modes are responsible for the temperature dependence of T_1 in other amorphous solids, as is presently thought to be the case, then the T_1 results in a-As provide evidence for the presence of tunneling modes in this solid as well. This result is particularly significant in view of the fact that no linear term in the low-temperature specific heat[10] is observed in a-As. The specific-heat results imply that the density of tunneling modes with energy differences $\lesssim 10^{-4}$ eV ($\cong 1$ K$/k$) is about an order of magnitude less than in other amorphous solids.

The T_1 and specific-heat results in a-As are also suggestive of the importance of spin diffusion in the tunneling-mode system (or perhaps the nuclear-spin system) because the magnitudes of T_1 at any given temperature in As_2Se_3 (where a linear term in C_v is observed) and a-As are comparable. Without spin diffusion, it is difficult to explain comparable magnitudes for T_1 in As_2Se_3 and a-As when the densities of tunneling modes differ by at least an order of magnitude. More detailed theoretical studies of T_1, which include the effects of spin diffusion in the tunneling-mode systems, are indicated.

B. Spin-spin relaxation

In earlier pulsed measurements of ^{75}As in glassy and crystalline As_2S_3 and As_2Se_3, Rubinstein and Taylor[15] concluded that the magnitudes of T_2 in these solids ($T_2 \sim 600$ μsec) were consistent with those expected for a dipolar interaction between like nuclei. Although these authors utilized an axially symmetric expression due to Abragam and Kambe[51] to describe an admittedly anisotropic situation for crystalline As_2S_3 and As_2Se_3, this conclusion will probably not be altered by a consideration of departures from axial symmetry. Using the expression of Abragam and Kambe,[51] we obtain similar agreement with the measured value of T_2 for or-As (167 μsec) where all the arsenic sites represent mutually resonant spins. Because T_2 for a-As is similar (~200 μsec) to that observed in or-As, we conclude that in both of these solids the spin-spin relaxation rates are determined predominantly by dipole-dipole interactions between mutually resonant spins.

VI. LINE-SHAPE AND FREQUENCY ANALYSES

A. NQR line shape: Effects of outside atoms

Figure 5(a) shows the NQR line shape for a-As. As can be seen from this figure, the line shape is broad and quite asymmetric. It will now be shown that much of the width of the line, as well as the asymmetry, can be accounted for by orientational arrangements of atoms directly bonded to the central atom. (The term "central atom" will represent the atoms whose NQR frequency we are calculating; the term "outside atom" will refer in general to all atoms other than the central atom. The outside atoms of primary importance in the following calculations are those directly bonded to the central atom.)

Atoms surrounding the central atom can be

thought of as consisting of bonding, nonbonding, and antibonding electrons, core electrons and a nucleus. As we are interested in an elemental material and all sites are chemically equivalent, there is to first order no charge transfer from one atom to another; therefore we assume that the total charge on any atom must sum to zero. However, there will be a charge distribution, where the bonding, nonbonding, and antibonding electrons will be further from the nucleus, on the average, than the core electrons. This distribution of charge will create an additional electric-field gradient (EFG) at the site of the central atom, in addition to the EFG created by the electrons of the central atom itself. Normally, this effect would be ignored; however, for the case of ^{75}As, which has a large quadrupole moment ($Q = 0.29$ barn), as well as a large value of the Sternheimer antishielding factor ([$\gamma_\infty = -7.332$ (Ref. 52)]; the Sternheimer antishielding factor accounts for polarizations of the core electrons caused by charges outside the core[53]), it cannot be.

A calculation was performed to obtain an estimate of the contribution to the coupling constant from such an effect. All outside atoms were assumed to consist of five hydrogenlike $4s$ and $4p$ electrons (total charge: $-5e$) and a nuclear core with charge $+5e$. The five $4s$ and $4p$ electrons were assumed to be hybridized in a pyramidal structure, consisting of a lone-pair density of two electrons, and three bonds with one electron each (see Ref. 26 for a description of the hybridized wave functions). This hybridization scheme pulls the center of the electronic distribution away from the nuclear site in the direction of the lone-pair orbital. The additional EFG from a particular outside atom was then calculated by numerically integrating over the entire spatial distribution of the hybridized orbitals of the outside atom and subtracting the effects of the nuclear core.

For the case of rh-As, the above calculation was performed by summing the effects over 47 nearest-neighbor atoms. This resulted in a change in the coupling constant, $\Delta Q_{cc} = +6.77$ MHz. Since Q_{cc} will most likely be negative in As materials [a single unbalanced p electron results in $Q_{cc}^{at} = -412$ MHz (Ref. 27)], the change in resonant frequency is $\Delta\nu_Q = -3.38$ MHz. This value agrees remarkably well with the value obtained by Sharma[32] ($\Delta Q_{cc} = 2\Delta\nu Q = 6.74$ MHz), where he used the ionic-model calculations of the EFG of Taylor and Hygh.[54] Considering the vast differences in the models, the agreement must be fortuitous, but it does indicate that the calculated value of ΔQ_{cc} are correct to within a factor of 2 or 3. A similar calculation for or-As showed that $\Delta Q_{cc} = +6.43$ MHz, resulting in a $\Delta\nu_Q = -3.22$ MHz. In both cases, as is well known, the effects of the outside atoms are *not* responsible for most of the EFG; the predominant effect must come from the bonding and nonbonding electrons of the central atom.

The contribution to the EFG from outside atoms in a-As was obtained by varying the dihedral angle. (The dihedral angle is the angle of rotation along the As–As bond required to bring the pair into an eclipsed position.[1]) The change in coupling constant ΔQ_{cc} was calculated for 18 values of the dihedral angle; each value of the dihedral angle was appropriately weighted, and a histogram of ΔQ_{cc} as a function of intensity was constructed. This is shown in Fig. 5 for the dihedral angle distribution of Greaves and Davis.[24] (A similar dihedral angle distribution of Beeman and Alben[55] resulted in a similar NQR line shape.) Note that the model predicts the observed asymmetry in the NQR line shape. This asymmetry is due to the asymmetry of the dihedral angle distribution—a flat dihedral angle distribution results in a symmetric NQR line shape. The degree of asymmetry of the NQR line shape depends upon the asymmetry of the dihedral angle distribution—a steeper dihedral angle distribution results in a more asymmetric NQR line shape.

Note also that the calculation linewidth of the spectrum is about $\frac{1}{3}$ the width of the experimental spectrum. This lack of quantitative agreement could possibly come from several sources of error in the calculation: First of all, because we are concerned with various forms of solid As, the concept of hydrogenlike orbitals is at best an elementary approximation. Second, the values of the nuclear quadrupole moment and the Sternheimer antishielding factor are not well known; conservative estimates support that both are correct to only ±20%. Third, the effective Bohr radius of the hydrogenlike orbitals is difficult to estimate. We calculated the quantity to be $a_0 = 0.0467$ Å from hyperfine measurements of $\langle 1/r^3 \rangle$ [$\langle 1/r^3 \rangle = 51 \times 10^{24}$ cm^{-3} (Ref. 56)] for atomic ^{75}As. Comparison of calculated charge densities versus distance from the hydrogenlike orbitals described above and those of Golin and Stocco[57] for rh-As [who used orthogonalized plane wave (OPW) wave functions] indicate that the above value is too small: The value $a_0 = 0.047$ Å does not predict a large enough electron density near the midpoint of an As–As bond. Therefore one must conclude that these calculations are probably in error by a factor of 2 or 3. Since the value of a_0 used predicts a smaller charge density near the center of the As–As bond than the more accurate OPW wave functions, we must conclude that

the calculated effects are too small. In fact, if one arbitrarily increases a_0 to 0.07 Å, the resulting a-As calculated linewidth is doubled, and the charge-density distribution in rh-As becomes more realistic.

Therefore it can be seen that this very simple model for the effects of outside atoms on EFG's in a-As explains the observed asymmetry of the NQR line shape, and predicts, within a factor of 2 or 3, the correct linewidth. Hopefully this simple calculation will stimulate more sophisticated theoretical investigations.

B. NQR frequencies: Townes-Dailey model

It was noted in Sec. IV that, although the x-ray data indicated that the local structures of the three forms of As are similar, the NQR frequencies are quite different. We have just shown that this difference cannot arise from variations in the orientation of outside atoms; therefore the difference must arise from subtle changes in the local configurations of bonding and nonbonding electrons. The approach employed here is the simplest possible bond hybridization calculation (due to Townes and Dailey[58]).

For the case of a symmetric pyramidal bonding structure, the calculated frequency due only to bonding and nonbonding s and p electrons is given by[26]

$$\nu_Q^{at} = (Q_{cc}^0/2)(3\cos^2\theta - 1)/\sin^2\theta$$
$$= 3Q_{cc}^0 \cos\phi/(1-\cos\phi), \quad (7)$$

where Q_{cc}^0 is the coupling constant due to a single unpaired p electron ($Q_{cc}^0 = -412$ MHz),[27] θ is the pyramidal apex angle, and ϕ is the angle between the hybridized bonding electronic wave functions. Using the wave functions given in Ref. 26, the fractional s character is given by

$$s = (\tfrac{2}{3})\nu_Q^{at}/Q_{cc}^0 . \quad (8)$$

By assuming that the outside atoms contribute approximately -3 MHz to ν_Q, the fractional s character can be calculated and is given in Table II. Clearly, the different NQR frequencies lead to quite different estimates of the s character and bonding wave-function angle ϕ. Note that the angle ϕ is reasonably close to the x-ray value for the *actual bond angle* α (Table I) for a-As, but quite different for the two crystals. We attribute this discrepancy to the fact that the bonds in rh-As and or-As (and probably also a-As) do not have maximum overlap. Since bonding in this case results from a minimization of the energy for two processes—bond overlap, decreasing the energy, and s admixture, increasing the energy—the energy minimum may occur for angles of ϕ somewhat different from the bond angles derived from x-ray measurements.

TABLE II. Calculation of the fractional s character (s), the angle between the bonding wave functions (ϕ) from the observed resonant frequency in the three forms of As using Eqs. (7) and (8). The quantity ν_Q^{at} is the NQR frequency resulting from effects only associated with the bonding electrons.

Material	ν_Q (MHz)	ν_Q^{at} (MHz)	s	ϕ
rh-As	23.56	20.56	0.033	91.9°
or-As	46.32	43.32	0.070	94.7°
a-As	63.5	60.5	0.098	96.3°

The use of the symmetric pyramid for or-As, crystalline As_2S_3, or crystalline As_2Se_3 is less appropriate because the pyramids (from x-ray data[59]) are asymmetric. Therefore an asymmetric pyramidal calculation was performed (this is shown in the Appendix; an earlier calculation by Rubinstein and Taylor[15] contained several errors) the results of which are summarized in Table III for the situation where the wave functions are assumed to lie along the bond angle determined from x-ray diffraction studies. The quantity Δ is the net charge left in each bonding orbital of the As atom after charge transfer; this quantity was calculated using the electronegativity formula for percent ionic character of a bond due to Hannay and Smyth.[60] The quantities S_0, S_1, S_2, and S_3 are the fractional s characters of the lone-pair orbital and bonds 1, 2, and 3, respectively. As can be seen, calculated results are in very poor agreement with the experimental values. X-ray photoemission spectroscopy (XPS) work in As_2S_3, rh-As, and a-As (Ref. 61) has indicated that the s character of the bonds in all these materials is low. Therefore the Townes-Dailey calculation in conjunction with the x-ray determination of bond angles, indicates that the bonds do not have maximum overlap in the As_2S_3 and As_2Se_3 systems, just as was determined above for the various forms of As.

Several calculations were performed using the equations of the Appendix to check the effects of bond distortion. One set of calculations simulated the "pinching together" of two bonds while another set simulated one bond bending while keeping the other two in place. Both sets of calculations indicated that the *total* s character of the three bonds was very insensitive to any sort of distortion, but that the quadrupole coupling constant, on the other hand, was very sensitive to the value of apex angle θ, the type of distortion, and the magnitude of the distortion. We suggest that these results indicate that the Townes-Dailey calculation, when adjusted to fit the observed NQR frequency, may

TABLE III. Calculation of the resonant frequency ν_Q and fraction s character of the lone-pair orbital (S_0), and bonds 1 (S_1), 2 (S_2), and 3 (S_3) from the Townes-Dailey approach shown in the Appendix. The quantity Δ is the amount of charge left in an As bonding orbital, calculated from electronegativity considerations. The values of the angles used in the calculation were determined from the x-ray work of Goldstein (As_2S_3 and As_2Se_3) and Smith *et al.* (*or*-As).

Site	ν_Q (expt) (MHz)	ν_Q (calc)	Δ	S_0	S_1	S_2	S_3
or-As	46.32	76.1	1.000	0.631	0.239	0.065	0.065
As_2S_3 I	72.86	130.1	0.911	0.418	0.497	0.029	0.054
II	70.38	111.8	0.911	0.501	0.368	0.037	0.094
As_2Se_3 I	60.0	208.4	0.933	0.052	0.942	0.001	0.004
II	56.0	113.2	0.933	0.484	0.372	0.049	0.094

be a good indication of the average s-p hybridization but a very unreliable method of estimating details of the bonding wave functions such as asymmetries.

In conclusion, the Townes-Dailey calculations which employ x-ray bond angles to describe the bonding wave functions cannot be used with any degree of accuracy, even to predict trends. This is probably due to the fact that the actual bonds are not pointing directly at the bonding atom and that maximum overlap is not occurring. In fact, taken at face value, the Townes-Dailey calculations suggest that the s-p hybridization is small in all the arsenic and arsenic chalcogenide materials investigated. It should be pointed out that the NQR frequency is a very useful parameter: If one has the correct wave function, it is a simple task to calculate the NQR frequency. Thus the NQR frequency is a valuable constraint on theoretical calculations. Hopefully, this fact will encourage more sophisticated theoretical investigations into the detailed electronic structure of these materials.

C. Temperature dependence of NQR frequencies

In a-As the NQR line shape is so broad that any temperature dependence of the peak frequency is unobservable. However, in the two crystalline forms the temperature dependence is easily measurable (see Ref. 32 and Fig. 7 for *rh*-As and *or*-As, respectively) and well fit by the Bayer model described in Sec. IV. The oscillator frequencies obtained for *rh*- and *or*-As using Eq. (6) are approximately 175 and 85 cm^{-1}, respectively. It is interesting to note that the lowest-energy peaks in the phonon spectra obtained from neutron scattering experiments[4] occur at ~100 and ~50 cm^{-1} for *rh*- and *or*-As, respectively. These values agree remarkably well with the predictions of the simple Bayer model. We conclude that the Bayer model provides a good, albeit elementary, picture of the influence of vibrational degrees of freedom on the temperature dependence of the NQR frequencies in these two elemental compounds.

VII. SUMMARY

Pulsed nuclear quadrupole resonance NQR measurements have been performed in the three forms of elemental arsenic: (1) the amorphous (a) semiconducting phase, (2) the semimetallic rhombohedral (*rh*) phase, and (3) the semiconducting orthorhombic (*or*) phase. The measurements included: (1) spin-lattice relaxation times (T_1) and spin-spin relaxation times (T_2) as functions of temperature in all three materials (the T_1 vs T for *rh*-As was reported in Ref. 31), (2) the NQR frequency (ν_Q) as a function of temperature (the ν_Q vs T for *rh*-As was reported by Sharma[32]), (3) T_1 and T_2 as a function of ν_Q at 77 K for a-As, and (4) the NQR line shape at 4.2, 77, and 300 K for all three forms.

It was found that $T_1 \propto T^{-1.5}$ in a-As; this dependence has been interpreted as evidence for the existence of tunneling or disorder modes in this material. This result is surprising in that the normal technique for determining the existence of disorder modes (observing a term linear with temperature in the low-temperature specific heat) indicated a much smaller density of these modes in a-As than in many other amorphous materials. Spin diffusion is invoked as a possible explanation of the discrepancy between these two experiments.

The NQR line shape of a-As was found to be highly asymmetric, with a full width at half maximum of 9 MHz. This asymmetry is probably due to a distribution of dihedral angles. A simple calculation was presented to demonstrate this possibility.

The observed NQR frequencies for the three forms of arsenic have been interpreted using the Townes-Dailey[58] model. The results show that

there are differing amounts of s admixture in the bonding wave functions of the three forms of arsenic (rh-As:3%, or-As:7%, a-As:10%) and that the bonding configurations do not correspond to maximum overlap of hybridized bonding orbitals on adjacent atoms.

ACKNOWLEDGMENTS

The authors are indebted to J. S. Lannin, A. J. Leadbetter, and the Smithsonian Institution for the loan of several samples of or-As, and to D. Beeman and W. A. Phillips for results prior to publication. The efforts of M. Rubinstein during the early stages of this work are greatly appreciated. One of the authors (G.E.J.) acknowledges the NRC/NRL Postdoctoral Research Associateship Program for support.

APPENDIX

A previous Townes-Dailey calculation performed by Rubinstein and Taylor[15] contained several errors (typographical and otherwise) which are corrected in this Appendix. The coordinate system used here is rotated about the z axis by 180° from that used in Ref. 15. We assume the following wave functions: four directed orbitals, three bonds, and one lone pair, hybridized from the neutral configuration (in As, the neutral configuration is $4s^24p^3$). Furthermore, we assume that the apex angle θ is the same for all three bonds (this assumption is equivalent to assuming that the bond lengths are all the same). The angles δ, γ, and ϵ are defined with respect to the bond projections onto the plane connecting the three outside atoms. The angle δ is the counterclockwise angle from bond 1 to bond 2, γ is the counterclockwise angle from bond 1 to bond 3, and ϵ is the clockwise angle from bond 1 to bond 3 (i.e., $\epsilon = 360° - \gamma$). The four wave functions are given by

$$
\begin{aligned}
\psi_0 &= S\phi_s + (1-S^2)^{1/2}(a\phi_z + b\phi_x + c\phi_y)\,,\\
\psi_1 &= S_1\phi_s + (1-S_1^2)^{1/2}(\phi_z\cos\theta + \phi_x\sin\theta)\,,\\
\psi_2 &= S_2\phi_s + (1-S_2^2)^{1/2}(\phi_z\cos\theta + \phi_x\sin\theta\cos\delta\\
&\qquad + \phi_y\sin\theta\sin\delta)\,,\\
\psi_3 &= S_3\phi_s + (1-S_3^2)^{1/2}(\phi_z\cos\theta + \phi_x\sin\theta\cos\gamma\\
&\qquad + \phi_y\sin\theta\sin\gamma)\,.
\end{aligned}
\tag{A1}
$$

Normalization requires that $a^2+b^2+c^2=1$. The orthogonalization of these wave functions yields

$$
\begin{aligned}
u_1 &= S_1^2/(1-S_1^2) = -[(\cos^2\theta + \sin^2\theta\cos\gamma)/(\cos^2\theta + \sin^2\theta\cos\epsilon)](\cos^2\theta + \sin^2\theta\cos\delta)\,,\\
u_2 &= S_2^2/(1-S_2^2) = -[(\cos^2\theta + \sin^2\theta\cos\delta)/(\cos^2\theta + \sin^2\theta\cos\gamma)](\cos^2\theta + \sin^2\theta\cos\epsilon)\,,\\
u_3 &= S_3^2/(1-S_3^2) = -[(\cos^2\theta + \sin^2\theta\cos\epsilon)/(\cos^2\theta + \sin^2\theta\cos\delta)](\cos^2\theta + \sin^2\theta\cos\gamma)\,.
\end{aligned}
\tag{A2}
$$

$$
a = c\tan\theta\left(\frac{\sin\delta(u_3/u_1 - \cos\gamma) - \sin\gamma(u_2/u_1 - \cos\delta)}{(u_2/u_1 - \cos\delta)(u_3/u_1 - 1) - (u_3/u_1 - \cos\gamma)(u_2/u_1 - 1)}\right),
$$

$$
b = c\left(\frac{\sin\delta(u_3/u_1 - 1) - \sin\gamma(u_2/u_1 - 1)}{(u_2/u_1 - \cos\delta)(u_3/u_1 - 1) - (u_3/u_1 - \cos\gamma)(u_2/u_1 - 1)}\right),
$$

$$
u^2 = S^2/(1-S^2) = -(a\cos\theta + b\sin\theta)/u_1\,.
$$

By choosing the sign of c to be positive, $c = (1-a^2-b^2)^{1/2}$.

We can now calculate the elements of the electric-field-gradient tensor by the equation

$$
q_{ij} = q_0^{\rm at}\sum_{k=0}^{3} e_i\langle\psi_k\,|\,L^{ij}\,|\,\psi_k\rangle\,,
\tag{A3}
$$

where L^{ij} is calculated using the Wigner-Eckart theorem and is given by

$$
L^{ij} = \tfrac{1}{2}[-\tfrac{3}{2}(l_il_j + l_jl_j) + \delta_{ij}l(l+1)]\,,
\tag{A4}
$$

where the l_i are angular momentum operators within the $L=1$ manifold for p electrons. In Eq. (A3), q_0^{at} is the electric-field gradient from a single unbalanced p electron, and e_i is the occupation of the ith orbital. The resulting 3×3 matrix for the EFG is given by

$$
q_{yx} = q_{xy} = \tfrac{3}{2}q_0^{at}[e_0(1-S^2)bc + e_2(1-S_2^2)\sin^2\theta\cos\delta\sin\delta + e_3(1-S_3^2)\sin^2\theta\cos\gamma\sin\gamma]\,,
\tag{A5}
$$

$$
q_{zx} = q_{xz} = \tfrac{3}{2}q_0^{at}[e_0(1-S^2)ab + e_1(1-S_1^2)\cos\theta\sin\theta + e_2(1-S_2^2)\sin\theta\cos\theta\cos\delta + e_3(1-S_3^2)\sin\theta\sin\theta\cos\gamma]\,,
\tag{A6}
$$

$$
q_{zy} = q_{yz} = \tfrac{3}{2}q_0^{at}[e_0(1-S^2)ac + e_2(1-S_2^2)\sin\theta\cos\theta\sin\delta + e_3(1-S_3^2)\sin\theta\cos\theta\sin\gamma]\,,
\tag{A7}
$$

$$q_{xx}=q_0\{(e_0/2)(1-S^2)(3b^2-1)+e_1(1-S_1^2)(\sin^2\theta-\cos^2\theta/2)$$
$$+e_2(1-S_2^2)[\sin^2\theta(\cos^2\delta-\sin^2\delta/2)-\cos^2\theta/2]+e_3(1-S_3^2)[\sin^2\theta(\cos^2\gamma-\sin^2\gamma/2)-\cos^2\theta/2]\}\,, \tag{A8}$$

$$q_{yy}=q_0\{(e_0/2)(1-S^2)(2-3a^2-3b^2)-(e_1/2)(1-S_1^2)$$
$$+e_2(1-S_2^2)[\sin^2\theta(\sin^2\delta-\cos^2\delta/2)-\cos^2\theta/2]+e_3(1-S_3^2)[\sin^2\theta(\sin^2\gamma-\cos^2\gamma/2)-\cos^2\theta/2]\}\,, \tag{A9}$$

$$q_{zz}=q_0\{(e_0/2)(1-S^2)(3a^2-1)+(\cos^2\theta-\sin^2\theta/2)[e_1(1-S_1^2)+e_2(1-S_2^2)+e_3(1-S_3^2)]\}\,. \tag{A10}$$

This matrix can then be diagonalized with diagonal components q_{xx}, q_{yy}, q_{zz}, and the NQR frequency is given by

$$\nu=\tfrac{1}{2}(e^2Qq_0/h)(1-\eta^2/3)^{1/2}\,, \tag{A11}$$

where the asymmetry parameter is given by

$$\eta=(q_{xx}-q_{yy})/q_{zz}\,. \tag{A12}$$

---

*Operated by Union Carbide Corporation for the U. S. Department of Energy under Contract No. W-7405-eng-26.

[1]G. N. Greaves, S. R. Elliott, and E. A. Davis, Adv. Phys. 28, 49 (1979).
[2]G. Lucovsky and J. C. Knights, Phys. Rev. B 10, 4324 (1974).
[3]J. S. Lannin, Phys. Rev. B 15, 3863 (1977); *Structure and Excitation of Amorphous Solids* in Proceedings of an International Conference on Structure and Excitation of Amorphous Solids, edited by G. Lucovsky and F. L. Galeener (AIP, New York, 1976), p. 123.
[4]A. J. Leadbetter, D. M. Smith, and P. Seyfert, Philos. Mag. 33, 441 (1976).
[5]F. Al-Berkdar, P. C. Taylor, G. D. Holah, J. G. Crowder, and C. R. Pidgeon, in *Amorphous and Liquid Semiconductors*, edited by W. E. Spear (University of Edinburgh, Edinburgh, 1977), p. 184.
[6]P. C. Taylor, S. G. Bishop, D. L. Mitchell, and D. Treacy, in *Proceedings of the Fifth International Conference on Amorphous and Liquid Semiconductors*, edited by J. Stuke and W. Brenig (Taylor and Francis, London, 1973), p. 1267.
[7]G. Lucovsky, Phys. Rev. B 6, 1480 (1972).
[8]R. C. Zeller and R. O. Pohl, Phys. Rev. B 4, 2029 (1971).
[9]C. N. King, W. A. Phillips, and J. P. de Neufville, Phys. Rev. Lett. 32, 538 (1974).
[10]D. P. Jones, N. Thomas, and W. A. Phillips, Philos. Mag. B 38, 271 (1978).
[11]Preliminary results were presented by G. E. Jellison, Jr., G. L. Petersen, and P. C. Taylor, Phys. Rev. Lett. 42, 1413 (1979).
[12]S. G. Bishop, U. Strom, and P. C. Taylor, Solid State Commun. 18, 573 (1977).
[13]P. C. Taylor, E. J. Friebele, and S. G. Bishop, Solid State Commun. 28, 247 (1978).
[14]R. J. Nemanich, G. Lucovsky, W. B. Pollard, and J. D. Joannopoulos, Solid State Commun. 26, 137 (1978).
[15]M. Rubinstein and P. C. Taylor, Phys. Rev. B 9, 4258 (1974).
[16]J. Szeftel and H. Alloul, Phys. Rev. Lett. 34, 657 (1975).
[17]M. Rubinstein, H. A. Resing, T. L. Reinecke, and K. L. Ngai, Phys. Rev. Lett. 34, 1444 (1975).
[18]T. L. Reinecke and K. L. Ngai, Phys. Rev. B 12, 3476 (1975).
[19]J. Szeftel and H. Alloul, J. Non-Cryst. Solids 29, 253 (1978).
[20]J. Szeftel and H. Alloul, Phys. Rev. Lett. 42, 1691 (1979).
[21]See, for example, A. Abragam, *The Principles of Nuclear Magnetism* (Clarendon, Oxford, 1961).
[22]R. W. G. Wyckoff, *Crystal Structures*, 2nd ed. (Wiley, New York, 1963), Vol. I.
[23]P. M. Smith, A. J. Leadbetter, and A. J. Apling, Philos. Mag. 31, 57 (1975).
[24]G. N. Greaves and E. A. Davis, Philos. Mag. 29, 1201 (1973); in *Proceedings of the Twelfth International Conference on Physics of Semiconductors, Stuttgart*, 1974 (Teubner, Stuttgart, 1974), p. 1047.
[25]W. Matthews, E. A. Davis, and S. R. Elliott (unpublished).
[26]T. P. Das and E. L. Hahn, *Nuclear Quadropole Resonance Spectroscopy*, Solid State Physics Suppl. 1 (Academic, New York, 1958).
[27]E. A. C. Lucken, *Nuclear Quadrupole Coupling Constants* (Academic, London, 1969).
[28]E. L. Hahn and B. Herzog, Phys. Rev. 93, 639 (1954).
[29]B. Herzog and E. L. Hahn, Phys. Rev. 103, 148 (1956).
[30]S. Alexander and A. Tzalmona, Phys. Rev. 138, A845 (1965).
[31]G. E. Jellison, Jr. and P. C. Taylor, Solid State Commun. 27, 1025 (1978).
[32]S. N. Sharma, Phys. Lett. 57A, 379 (1976).
[33]T. J. Bastow and H. J. Whitfield, Solid State Commun. 18, 955 (1976).
[34]N. Morimoto, Minerol. J. 1, 160 (1954).
[35]A. C. Renninger and B. L. Averbach, Acta Crystallogr. B 29, 1583 (1973).
[36]H. Bayer, Z. Phys. 130, 227 (1951).
[37]J. Van Kronendonk, Physica 20, 781 (1954).
[38]K. R. Jeffrey and R. L. Armstrong, Phys. Rev. 138, A 845 (1965); R. L. Armstrong and K. R. Jeffrey, Can. J. Phys. 47, 2165 (1968).

[39]G. E. Jellison, Jr., Solid State Commun. 30, 481 (1979).
[40]J. Haupt and W. Müller-Warmuth, Z. Naturforsch. 239, 208 (1968); 249, 1066 (1969).
[41]R. B. Stevens, Phys. Rev. B 8, 2896 (1973).
[42]U. Strom and P. C. Taylor, Phys. Rev. B 16, 5512 (1977).
[43]J. S. Lannin, H. F. Eno, and H. L. Luo, Solid State Commun. 25, 81 (1978).
[44]B. Golding, J. E. Graebner, B. I. Halperin, and R. J. Schutz, Phys. Rev. Lett. 30, 223 (1973); S. Hunklinger, W. Arnold, S. Stein, R. Nava, and K. Dransfeld, Phys. Lett. A 42, 253 (1972).
[45]M. Von Schickfus and S. Hunklinger, Phys. Lett. 64A, 144 (1977).
[46]P. W. Anderson, B. I. Halperin, and C. M. Varma, Philos. Mag. 25, 1 (1972).
[47]W. A. Phillips, J. Low Temp. Phys. 7, 351 (1972).
[48]L. Lyo and R. Orbach (unpublished).
[49]J. L. Block and B. I. Halperin, Phys. Rev. B 16, 2879 (1977).
[50]B. Golding and J. E. Graebner, Phys. Rev. Lett. 37, 852 (1976).
[51]A. Abragam and K. Kambe, Phys. Rev. 91, 894 (1953).
[52]F. D. Feilock and W. R. Johnson, Phys. Rev. 187, 39 (1969).
[53]R. M. Sternheimer, Phys. Rev. 80, 102 (1950).
[54]T. T. Taylor and E. H. Hygh, Phys. Rev. 129, 1193 (1963).
[55]D. Beeman and R. Alben, Adv. Phys. 26, 339 (1977).
[56]R. G. Barnes and W. V. Smith, Phys. Rev. 93, 95 (1954).
[57]S. Golin and J. A. Stocco, Phys. Rev. B 1, 390 (1970).
[58]C. H. Townes and B. P. Dailey, J. Chem. Phys. 17, 782 (1949).
[59]P. Goldstein (private communication); A. A. Vaipolin, Kristallografiya 10, 596 (1965).
[60]N. B. Hannay and C. P. Smyth, J. Am. Chem. Soc. 68, 171 (1946).
[61]S. G. Bishop and N. J. Shevchik, Phys. Rev. B 12, 567 (1975).